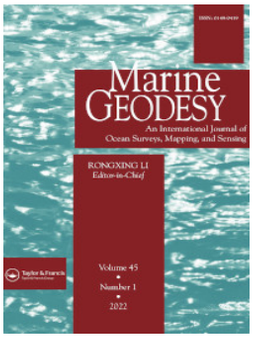

Marine Geodesy

ISSN: (Print) (Online) Journal homepage: https://www.tandfonline.com/loi/umgd20

# Establishing a Marine Gravity Database around Egypt from Satellite Altimetry-Derived and Shipborne Gravity Data

Ahmed Zaki, Mahmoud Magdy, Mostafa Rabah & Ahmed Saber

**To cite this article:** Ahmed Zaki, Mahmoud Magdy, Mostafa Rabah & Ahmed Saber (2021): Establishing a Marine Gravity Database around Egypt from Satellite Altimetry-Derived and Shipborne Gravity Data, Marine Geodesy, DOI: 10.1080/01490419.2021.2020185

**To link to this article:** https://doi.org/10.1080/01490419.2021.2020185

Published online: 30 Dec 2021.

MARINE GEODESY
https://doi.org/10.1080/01490419.2021.2020185

Taylor & Francis
Taylor & Francis Group



# Establishing a Marine Gravity Database around Egypt from Satellite Altimetry-Derived and Shipborne Gravity Data

Ahmed Zaki[a], Mahmoud Magdy[b], Mostafa Rabah[b], and Ahmed Saber[b]

[a]Civil Engineering Department, Faculty of Engineering, Delta University for Science and Technology, Gamasa, Egypt; [b]Department of Civil Engineering, Benha Faculty of Engineering, Benha University, Benha, Egypt

**ABSTRACT**

For the purpose of marine geoid modeling and many other geodetic and geophysical applications, a marine gravity map around Egypt is established by the integration of gravity data provided by satellite altimetry and shipborne gravimetric observations. Firstly, the collected shipborne data were compared with GO_CONS_GCF_2_TIM_R6 and XGM2019e GGMs and with SSv29.1 and DTU17 altimetry models. Then, a pre-refinement of ship marine surveys was done with a rigorous condition, in which a number of 6525 points have been removed from the dataset. After that, 87709 points were deducted from the pre-filtered shipborne dataset to fit the study area and the cross-validation approach with the kriging interpolation algorithm were applied. A rigorous level of confidence was decided in this step where the points which have differences between the estimated and the observed values more than twice the STD of the residuals were removed until the STD reached a value less than 1 mGal. Finally, the filtered shipborne gravity data were combined with DTU17 (the best evaluation model) using the least-squares collocation technique (LSC). The final gravity map was tested using 8000 randomly chosen shipborne stations, which were not included when applying LSC, revealing the significant enhancement gained after the integration process.

**ARTICLE HISTORY**
Received 30 August 2021
Accepted 13 December 2021

**KEYWORDS**
Egypt; global geopotential models (GGM); Marine gravity; satellite altimetry; shipborne gravity

## Introduction

Gravity anomalies are important for several applications in geophysics and geodesy such as studying sub-surface geological structure, offshore investigations, and tectonics (Hackney and Featherstone 2003). In addition, the gravity anomalies can be used to the determination of the geoid model (Hackney and Featherstone 2003), constructing high-resolution global gravity models for climate studying (Andersen, Knudsen, and Berry 2010; Liu

**CONTACT** Mahmoud Magdy mahmoud.fouad@bhit.bu.edu.eg Department of Civil Engineering, Benha Faculty of Engineering, Benha University, Benha, Egypt

et al. 2016). In the ocean, gravity anomalies are regarded as vital information for exploring the ocean (Fairhead, Green, and Odegard 2001), studying seafloor topography (D. T. Sandwell et al. 2014; Y. Zhang et al. 2003), shipborne surveys planning (Gaina et al. 1998), tectonics studies (Haxby et al. 1983), and petroleum explorations and inertial navigation (D. T. Sandwell and Smith 1997).

Establishing an accurate and high-resolution marine gravity field over a certain area cannot be done using one source of gravity data, as each data source has different parameters and represents the gravity field in a certain spectrum (in a certain range of wavelength). This means that the best way to create a marine gravity map, completely and accurately representing the entire spectrum of the gravity field in a certain area, is to combine heterogeneous and disparate gravity datasets from different sources, e.g., global geopotential models (GGMs), altimetry-derived models, and shipborne observations. Global geopotential models (GGMs) provide global homogeneous coverage of the gravity field over the Earth based on satellite gravimetry observations. Such models describe the long-wavelength characteristics of the gravity field and are called satellite-only GGMs, e.g., GO_CONS_GCF_2_TIM_R6 GGM (Brockmann et al. 2019). Satellite gravimetry observations can be combined with terrestrial data and other data sources resulting in so-called combined GGMs. These combined models can improve the medium-to-short wavelength characteristics of the gravitational field, an example of the combined models used in our study is XGM2019e GGM (Zingerle et al. 2020).

On the other hand, the satellite altimetry-derived models like DTU17 (Andersen and Knudsen 2019) global gravity field model and its predecessors, released by the Technical University of Denmark (DTU), and the Sandwell and Smith gravity model (SSv29.1) (David T. Sandwell et al. 2021) as well as its predecessors, released by the Scripps Institution of Oceanography (SIO), permit homogeneous and dense global mapping of short-wavelength gravity signals, where the offshore gravity data are delivered by the observations from various satellite altimetry missions and the onshore free-air gravity data are provided by the Earth Geopotential Model 2008 (EGM 2008) (Pavlis et al. 2012). However, the accuracy of the altimetric observations decreases near coasts and in shallow water. This is due to the poor modeling of tides near coasts, the high variability of the sea surface, and the loss of tracking of the altimeter due to onshore reflector interference (Christensen and Andersen 2016).

Finally, there are shipborne gravity data, the most direct measurement approach of gravity in marine areas. However, unfortunately, such data provide local coverage of the gravity field. Shipborne gravimetric observations can provide a significant enhancement of the short-wavelength signals

especially in shallow water and coastal zones where the altimetric data accuracy deteriorates. However, it may include biases due to more types of errors such as navigational errors, instrumental errors, and other sources of errors (Wessel and Watts 1988). Hence, this paper aims to evaluate and validate the shipborne gravity data using the other data sources as reference data and the specified techniques, then apply the best possible enhancement of these data by integrating them to finally obtain a high-resolution and accurate marine gravity field around Egypt, which in turn can be utilized to estimate a high-resolution marine geoid and also can provide essential contributions for other geodetic and geophysical applications. Section "Gravity datasets" describes the different gravity data sources used in our study. The evaluation of the shipborne gravity dataset by the other data sources is presented in section "Evaluation of shipborne data". Then the validation and filtering of shipborne data are performed in section "Filtering shipborne data". Finally, section "Integration of DTU17 grid and refined shipborne data" presents the integration of shipborne and altimetry-derived gravity data.

## Gravity datasets

### *Global geopotential models (GGMs)*

Global Geopotential Models (GGMs) are used to describe the gravity potential (geopotential) of the Earth expressed in terms of a series of spherical harmonic coefficients, outside of the attracting masses of the Earth, providing information for the lower degree components (long-wavelength characteristics) of the gravity field (Omar, Ses, and Mohamed 2005).

Three types of gravity field models are provided on the website of the International Centre for Global Earth Models (ICGEM) (http://icgem.gfz-potsdam.de/) (Ince et al. 2019): static models, temporal models, and topographic gravity field models. In this study, we have utilized the latest two available satellite-only and combined static models having maximum degree and order (d/o) for the evaluation of the shipborne gravity data, i.e., the satellite-only GO_CONS_GCF_2_TIM_R6 model with d/o 300 (Brockmann et al. 2019), and the combined XGM2019e model with d/o 2190 (Zingerle et al. 2020).

#### *Go_CONS_GCF_2_TIM_R6 model*

GO_CONS_GCF_2_TIM_R6 (see Figure 1 - panel a), represented as a spherical harmonic expansion with maximum degree 300, reflects the Earth's gravity field in the long-term based on the observations from the Gravity field and steady-state Ocean Circulation Explorer (GOCE) satellite

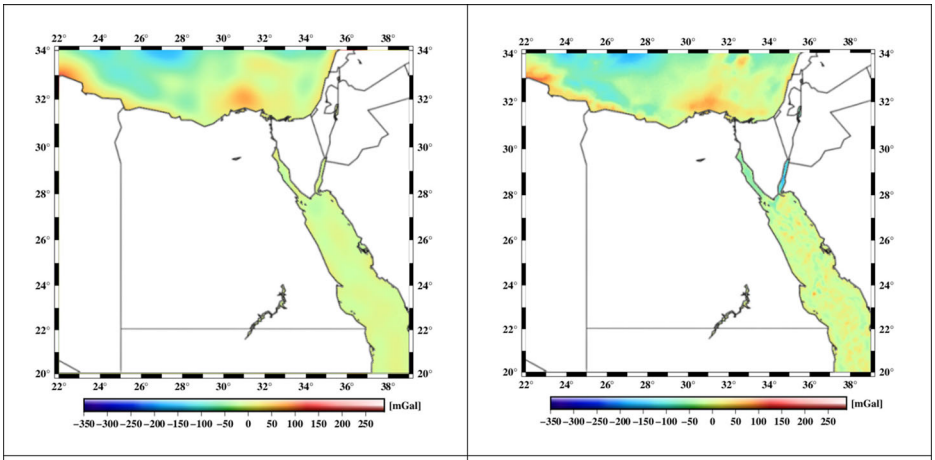


**Figure 1.** Free-air gravity anomalies from GO_CONS_GCF_2_TIM_R6 model (panel a), and XGM2019e model (panel b) around Egypt; units [mGal]. Source: Author.

mission (Drinkwater et al. 2003), launched on March 17, 2009, by the European Space Agency (ESA). For the data processing, the official ESA GOCE High-level processing facility (GOCE-HPF) pursues three approaches: (1) the space-wise approach, (2) the direct approach, and (3) the time-wise approach (Pail et al. 2011).

GO_CONS_GCF_2_TIM_R6 is the 6th release of the GOCE gravity field model by means of the time-wise approach (Brockmann et al. 2019). Such an approach avoids the usage of any observations of the gravity field except the GOCE data. Thus, it is a good fit for the combination of different observation types and represent the gravity field of the Earth as observed by GOCE. As the data processing of a single mission beginning at the observation level, consistency is ensured and strict modeling of the errors from the observations to the final model estimation is realized. This led to the second request to the time-wise models, that is to provide a realistic error description of the model in terms of a full covariance matrix (Brockmann, Schubert, and Schuh 2021). For a GOCE-only model, to accomplish a respectable performance of the entire spherical harmonics' spectrum, it is necessary to combine a gravity field estimated from good quality gravity gradients and kinematic orbits. Moreover, due to the polar gap (Rudolph, Kusche, and Ilk 2002; Sneeuw and van Gelderen 1997), some mathematical regularization has to be applied to constrain the data gaps and to enhance the signal-to-noise ratio for high degrees.

### *XGM2019e model*

XGM2019e (see Figure 1 - panel b), published in 2019, is represented by spheroidal harmonics up to degree and order (d/o) 5399, corresponding to

a spatial resolution of 2′ (∼ 4 km at the equator). Since the release of EGM2008 by the National Geospatial-Intelligence Agency in 2008 (Pavlis et al. 2012) till 2019, Only three gravity models were represented by spherical harmonics with maximum d/o larger than 2000, i.e., EIGEN-6C4 in 2014 (Förste et al. 2014), GECO in 2015 (Gilardoni, Reguzzoni, and Sampietro 2016), and SGG-UGM-1 in 2018 (Wei et al. 2018). All these models mainly used EGM2008 as a data source above the resolution of satellite-only models and consequently are highly dependent on that model (Zingerle et al. 2020).

XGM2019e differs from the preceding ones as it is independent of EGM2008. It mainly uses a combination of three data sources: the satellite-only model GOCO06s (Kvas et al. 2021) in the longer-wavelength range up to d/o 300 combined with a grid of ground gravity data that covers the shorter wavelengths. The ground data over land and ocean provided by the US National Geospatial-Intelligence Agency (NGA) with 15′ resolution (∼ 30 km at the equator), identical to XGM2016 (Pail et al. 2018) augmented with gravity information derived from topography data over land EARTH2014 (Rexer, Hirt, and Pail 2017). Over the oceans, gravity anomalies derived from satellite altimetry are used (DTU13) (Andersen et al. 2013) with a resolution of 1′ (∼ 2 km at the equator). The combination of the data from the satellite with the ground observations is performed using full normal equations up to d/o 719 (15′). Beyond d/o 719, a block-diagonal least-squares solution is computed for the ground gravity data of high resolution (from topography and altimetry). Three different spectral resolutions of the model are available on ICGEM: d/o 5540, 2190, and 760, the model with d/o 2190 is used in our study.

### *Altimetry derived gravity models*

Here we use the latest published and the most well-known altimetry-derived gravity models for the evaluation process. The DTU17 (Andersen and Knudsen 2019) global gravity field model, released by the Technical University of Denmark (DTU) and the Sandwell and Smith gravity model (SSv29.1) (David T. Sandwell et al. 2021), released by the Scripps Institution of Oceanography (SIO). These derived gravity models are mainly based on the Jason-1/2 end of life, CryoSat-2, and SARAL/AltiKa geodetic missions. Jason-1 (2001-2013) completes one geodetic mission cycle in ∼406 days with track spacing reaches ∼ 8 km at the equator. while Jason-2 (2008-2019) conducted two complete long repeat orbit (LRO) cycles in ∼371 days with track spacing of around 4–5 km. Cryosat-2, launched in April 2010, also provides high-quality sea surface height

**Table 1.** General information of the altimetric geodetic missions.

| Geodetic mission | GM repeat cycle (days) | Altitude (km) | Inclination | Cross-track distance (km) |
|---|---|---|---|---|
| Jason-1 | 406 | 1336 | 66° | ~8 |
| Jason-2 | 371 | 1336 | 66° | 4-5 |
| CryoSat-2 | 369 | 717 | 92° | ~8 |
| SARAL/AltiKa | – | ~800 | 98.55° | – |

measurements with a repeating period of ~ 369 days and ~ 8 km cross-track sampling.

In 2016, a new geodetic mission SARAL/AltiKa become available. This mission provides two main enhancements of altimetry-derived gravity data, the first is the higher pulse repetition frequency (4000 Hz) as it operates at Ka-band, while other altimetric missions operate at Ku band with 2000 Hz pulse repetition frequency, generating a higher number of independent observations that can be averaged to improve the range precision. The second is that the altimeter using Ka-band has a smaller footprint that is good for coastal zones, as the small footprint permits lower corruption of sea surface height observations near land areas. Besides the four geodetic missions mentioned above, the involved gravity models i.e., DTU17 and SSv29.1 also adopted other altimetric datasets, e.g., Geosat GM/ERM, ERS GM/ERM, Envisat, T/P, and T/P retracked data (Andersen and Knudsen 2019). General information of the mentioned geodetic missions is listed in Table 1.

DTU17 and SSv29.1 are presented as grids with a resolution of 1 arc minute. For the marine gravity modeling from altimetric observations, DTU17 depends on geoid undulation [sea surface height approach (SSH)] (Andersen and Knudsen 2019). The relationship between marine gravity anomaly and geoid undulation is established by the inverse Stokes equation (Hofmann and Moritz 2006), while SSv29.1 utilizes vertical deflection [sea surface slope approach (SSS)] (D. T. Sandwell et al. 2013) and the marine gravity anomaly is obtained using Laplace equation (D. T. Sandwell and Smith 1997). Both methods apply Fast Fourier Transform (FFT) algorithms in the calculation under the flat earth approximation. When compared to the method of SSS, the SSH approach reveals a good performance over shallow water and near coastal areas as it is less affected by the lack of data on the land near coasts (Zaki and Mogren 2021). While the use of the SSS approach is better over the open ocean and also produces gravity anomalies that are noticeably richer in high-frequency content with respect to residual SSH (S. Zhang et al. 2021). On the other hand, the static combined global geopotential model EGM2008 with a maximum degree of 2190 is used to complete the free-air gravity data on land areas. The two altimetry derived models are presented in Figure 2.

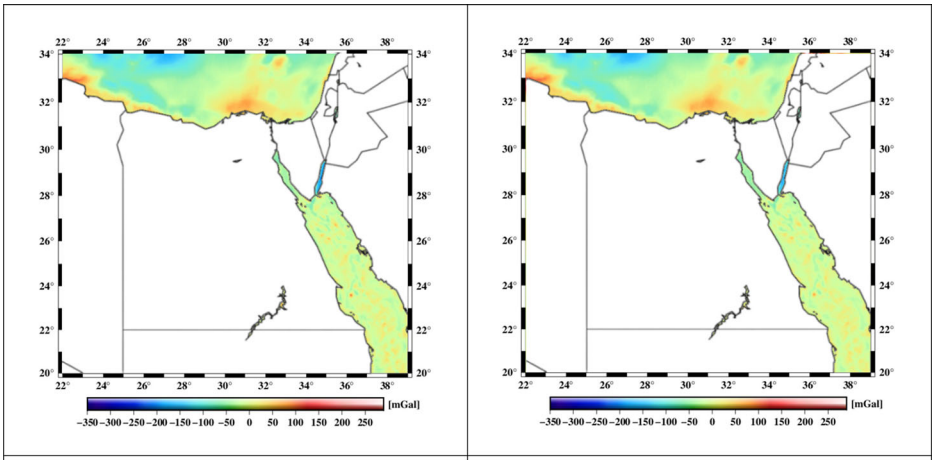


**Figure 2.** Free-air gravity anomalies from SSv29.1 model (panel a), and DTU17 model (panel b) around Egypt; units [mGal]. Source: Author.

### *Shipborne gravity data*

The shipborne gravity data were obtained from the National Geophysical Data Center (NGDC) (https://maps.ngdc.noaa.gov/viewers/geophysics/). Within a larger range of ($20° \leq$ lat $\leq 34°$; $22° \leq$ long $\leq 39°$) than the range of our study area of ($22° \leq$ lat $\leq 32°$; $24° \leq$ long $\leq 37°$), there are seventeen ship marine surveys from 1964 to 1988. The margins of 2 degrees from each border of the Egyptian borders were taken into account to decrease the effect of window distortion in the interpolation process. These marine surveys, passing through the study area, extend in geodetic latitude from (lat $= 11.61°$) to (lat $= 52.83°$) and in geodetic longitude from (long $= -68.74°$) to (long $= 44.89°$) with a total number of 161039 points having values range between $-775.80$ mGal and 890.00 mGal with a mean value of $-28.82$ mGal and a STD of 50.80 mGal, where no available metadata describing their accuracies. While the distribution of the data within the study area is uneven, where about 85% of the data exist in the Red Sea region while only ~15% of the data exist in the Mediterranean Sea region showing large gaps as presented in Figure 3.

The collected shipborne gravity data include biases that need to be overcome. These biases are due to types of errors such as navigational errors, e.g., positioning uncertainties and Eötvös effect, instrumental errors, e.g., gravimeter drift and cross-coupling, and other sources of errors, e.g., inconsistent datum, error in ties, and sea conditions (Wessel and Watts 1988). So, before integrating such data with any other gravity data sources, one should ensure that these data are consistent and outliers-free. In this investigation, every ship marine survey is independently evaluated by the

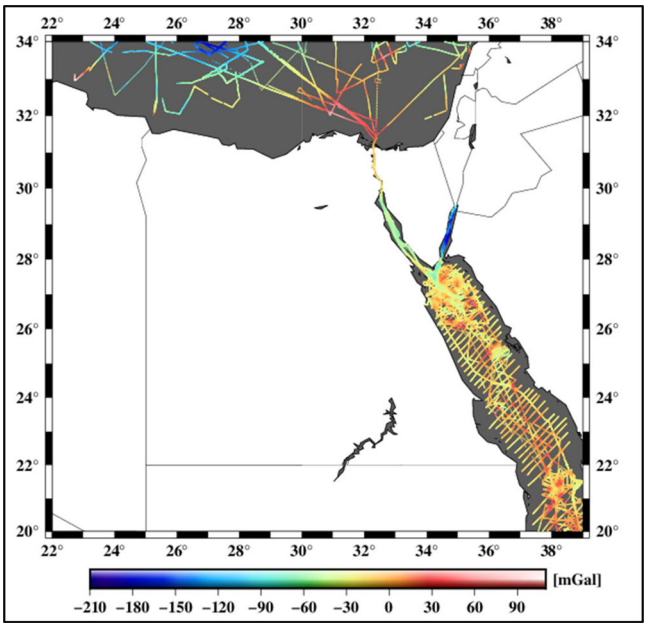


**Figure 3.** The distribution of the pre-refined shipborne data within the study area range; units [mGal]. Source: Author.

mentioned GGMs and altimetry-derived gravity models. Then a pre-refinement is done according to the best evaluation model that gives minimum statistics of the residuals. Finally, the data within the study area range were filtered using the cross-validation technique to fully remove the outliers and then can be combined with other data sources.

## Evaluation of shipborne data

### *Comparison of shipborne gravity data with GGMs*

In this section, it is decided to evaluate the whole track gravity data of each marine survey to make an overview of each track's accuracy before deducting the data needed for the study area. A number of 17 marine surveys were independently evaluated using the satellite-only GO_CONS_GCF_2_TIM_R6 GGM and the combined XGM2019e GGM. the former is based on the satellite gravimetry observations only from the GOCE satellite mission without any contribution of the shipborne gravity data or any other terrestrial data, providing precise information about long-wavelength characteristics of the Earth's gravitational field. The latter provides a detailed gravity field with better spatial resolution by integrating satellite gravimetry observations with ground, topography, and altimetry-derived gravity data. The statistics of the residuals between the gravity

**Table 2.** Evaluation of ship marine surveys by GO_CONS_GCF_2_TIM_R6 model; units [mGal].

| | | | Statistics of residuals | | | |
|---|---|---|---|---|---|---|
| Survey no | Survey name | No. of data | Min | Max | Mean | STD |
| 1 | 88004311 (1988) | 27346 | −106.26 | 103.80 | −5.03 | 18.18 |
| 2 | RC2507 (1984) | 38929 | −100.57 | 68.76 | −5.14 | 20.34 |
| 3 | 83005811 (1983) | 7561 | −143.94 | 84.33 | −5.37 | 21.43 |
| 4 | 83005911 (1983) | 7275 | −113.93 | 70.01 | −18.49 | 19.64 |
| 5 | 83008011 (1983) | 13447 | −133.90 | 65.99 | −14.83 | 17.47 |
| 6 | AKU30A (1979) | 842 | −87.02 | 36.69 | −10.38 | 15.76 |
| 7 | DI103B (1979) | 2293 | −237.38 | 46.78 | 9.19 | 17.94 |
| 8 | SHA1079 (1979) | 12194 | −770.16 | 120.46 | −0.99 | 36.32 |
| 9 | A2093L19 (1977) | 9638 | −191.76 | 285.44 | −58.96 | 67.04 |
| 10 | A2093L20 (1977) | 1499 | −37.92 | 40.44 | −2.60 | 13.46 |
| 11 | CH100L03 (1971) | 4096 | −37.53 | 51.85 | −0.81 | 14.56 |
| 12 | CH061L01 (1966) | 13948 | −109.75 | 154.01 | 3.02 | 30.32 |
| 13 | CH061L02 (1966) | 6806 | −108.59 | 162.04 | 6.97 | 23.12 |
| 14 | RC0911A (1965) | 752 | −75.04 | 47.21 | −9.17 | 17.76 |
| 15 | RC0911B (1965) | 967 | −66.68 | 73.68 | −3.72 | 23.14 |
| 16 | CH043L01 (1964) | 3798 | −114.14 | 873.92 | −9.30 | 25.31 |
| 17 | CH043L03 (1964) | 9648 | −150.70 | 70.54 | −12.82 | 27.04 |

**Table 3.** Evaluation of ship marine surveys by XGM2019 model; units [mGal].

| | | | Statistics of residuals | | | |
|---|---|---|---|---|---|---|
| Survey no | Survey name | No. of data | Min | Max | Mean | STD |
| 1 | 88004311 (1988) | 27346 | −72.38 | 55.52 | −4.06 | 3.71 |
| 2 | RC2507 (1984) | 38929 | −39.86 | 38.60 | −1.79 | 7.74 |
| 3 | 83005811 (1983) | 7561 | −51.35 | 40.83 | −1.12 | 5.78 |
| 4 | 83005911 (1983) | 7275 | −73.93 | 91.97 | −6.15 | 8.13 |
| 5 | 83008011 (1983) | 13447 | −111.79 | 68.91 | −9.84 | 7.89 |
| 6 | AKU30A (1979) | 842 | −41.66 | 17.73 | −12.78 | 9.71 |
| 7 | DI103B (1979) | 2293 | −269.70 | 34.67 | 8.81 | 11.37 |
| 8 | SHA1079 (1979) | 12194 | −766.38 | 50.25 | −0.49 | 32.54 |
| 9 | A2093L19 (1977) | 9638 | −62.16 | 317.29 | −10.58 | 15.27 |
| 10 | A2093L20 (1977) | 1499 | −21.66 | 15.65 | −2.25 | 4.62 |
| 11 | CH100L03 (1971) | 4096 | −24.33 | 47.79 | 2.23 | 6.08 |
| 12 | CH061L01 (1966) | 13948 | −87.80 | 144.93 | 5.14 | 10.20 |
| 13 | CH061L02 (1966) | 6806 | −32.61 | 52.76 | 10.57 | 9.56 |
| 14 | RC0911A (1965) | 752 | −29.90 | 14.12 | −6.80 | 6.95 |
| 15 | RC0911B (1965) | 967 | −44.42 | 25.56 | −3.10 | 6.13 |
| 16 | CH043L01 (1964) | 3798 | −61.16 | 886.17 | −9.57 | 18.69 |
| 17 | CH043L03 (1964) | 9648 | −94.49 | 48.28 | −10.33 | 13.63 |

observations of each survey and the two reference GGMs are shown in Tables 2 and 3, respectively.

### *Comparison of shipborne gravity data with altimetry derived models*

Satellite altimetry-derived marine gravity grids, i.e., DTU17 and SSv29.1 provide a global homogeneous coverage based on a combination of several satellite missions. However, the quality of the gravity data derived from altimetry is known to deteriorate in shallow water and near coasts, mainly due to high variability of the sea surface, loss of the altimeter tracking triggered by land reflector interference, and poor near-coast tidal models (Christensen and Andersen 2016). On the other hand, shipborne

**Table 4.** Evaluation of ship marine surveys by SSv29.1 model; units [mGal].

| | | | Statistics of residuals | | | |
|---|---|---|---|---|---|---|
| Survey no | Survey name | No. of data | Min | Max | Mean | STD |
| 1 | 88004311 (1988) | 27346 | −68.67 | 58.66 | −3.01 | 3.61 |
| 2 | RC2507 (1984) | 38929 | −32.47 | 37.58 | −0.85 | 4.99 |
| 3 | 83005811 (1983) | 7561 | −52.01 | 73.67 | 0.04 | 6.61 |
| 4 | 83005911 (1983) | 7275 | −90.47 | 93.88 | −6.26 | 7.81 |
| 5 | 83008011 (1983) | 13447 | −109.02 | 66.21 | −11.66 | 7.37 |
| 6 | AKU30A (1979) | 842 | −42.69 | 14.72 | −12.61 | 8.32 |
| 7 | DI103B (1979) | 2293 | −249.15 | 35.06 | 11.03 | 9.50 |
| 8 | SHA1079 (1979) | 12194 | −772.08 | 45.32 | 0.04 | 32.41 |
| 9 | A2093L19 (1977) | 9638 | −51.57 | 327.42 | 3.17 | 15.52 |
| 10 | A2093L20 (1977) | 1499 | −11.61 | 18.98 | −0.77 | 4.57 |
| 11 | CH100L03 (1971) | 4096 | −23.27 | 50.47 | 2.04 | 5.29 |
| 12 | CH061L01 (1966) | 13948 | −89.60 | 146.14 | 6.37 | 9.72 |
| 13 | CH061L02 (1966) | 6806 | −56.99 | 55.27 | 11.31 | 9.38 |
| 14 | RC0911A (1965) | 752 | −30.69 | 30.46 | −5.95 | 6.18 |
| 15 | RC0911B (1965) | 967 | −72.62 | 29.23 | −2.01 | 6.05 |
| 16 | CH043L01 (1964) | 3798 | −62.97 | 886.41 | −9.41 | 18.32 |
| 17 | CH043L03 (1964) | 9648 | −93.09 | 47.23 | −9.13 | 13.51 |

gravimetry is the most direct method of observing the gravity in marine areas, especially in regions where the quality of the altimetric data degrades. Therefore, such marine observations can play an important role to enrich the altimetric gravity signal in the short wavelength, especially for observations in harbors, ports, and near coasts (D. T. Sandwell et al. 2001), with a rigorous level of confidence in the outliers-removal step. Tables 4 and 5 show the results of the evaluation applied.

## *Results and discussion*

Table 6 summarizes the statistics of the residuals between the entire shipborne dataset and each reference gravity model after removing 1115 duplicated points caused by the intersection of marine surveys.

GO_CONS_GCF_2_TIM_R6 shows the worst results of the residuals with larger mean and STD of −8.35 mGal and 31.06 mGal, respectively, which demonstrate the lower spatial resolution of the gravity model and the large spectral gap between the model and the shipborne data. While XGM2019e model fit the shipborne data better than the satellite-only model reflecting the significant improvements of satellite gravimetry observations when integrated with other data sources, i.e., altimetry, ground, and topography data. On the other hand, it can be concluded that both altimetry-derived models demonstrate the best results when compared with the shipborne data. Hence, DTU17 was preferably exploited to complete the filtering and the integration with shipborne data for two reasons, the first is its low STD value of 12.95 mGal and the second is the algorithm employed to acquire the gravity data from altimetric observations, i.e., sea surface

**Table 5.** Evaluation of ship marine surveys by DTU17 model; units [mGal].

| | | | Statistics of residuals | | | |
|---|---|---|---|---|---|---|
| Survey no | Survey name | No. of data | Min | Max | Mean | STD |
| 1 | 88004311 (1988) | 27346 | −69.41 | 58.51 | −4.16 | 3.52 |
| 2 | RC2507 (1984) | 38929 | −24.98 | 38.06 | 0.25 | 5.72 |
| 3 | 83005811 (1983) | 7561 | −49.03 | 41.22 | −0.59 | 5.21 |
| 4 | 83005911 (1983) | 7275 | −86.61 | 87.60 | −6.51 | 7.52 |
| 5 | 83008011 (1983) | 13447 | −108.23 | 65.92 | −10.02 | 6.97 |
| 6 | AKU30A (1979) | 842 | −40.28 | 15.31 | −12.06 | 8.64 |
| 7 | DI103B (1979) | 2293 | −251.74 | 32.64 | 10.20 | 10.36 |
| 8 | SHA1079 (1979) | 12194 | −771.21 | 41.38 | 0.30 | 32.59 |
| 9 | A2093L19 (1977) | 9638 | −38.93 | 314.24 | −2.77 | 9.69 |
| 10 | A2093L20 (1977) | 1499 | −17.30 | 20.29 | −1.40 | 5.34 |
| 11 | CH100L03 (1971) | 4096 | −23.52 | 43.89 | 1.74 | 5.69 |
| 12 | CH061L01 (1966) | 13948 | −88.12 | 144.12 | 5.47 | 9.82 |
| 13 | CH061L02 (1966) | 6806 | −36.95 | 48.58 | 11.14 | 9.24 |
| 14 | RC0911A (1965) | 752 | −24.36 | 11.83 | −5.90 | 6.34 |
| 15 | RC0911B (1965) | 967 | −50.73 | 21.76 | −2.79 | 5.72 |
| 16 | CH043L01 (1964) | 3798 | −63.54 | 885.12 | −9.36 | 18.43 |
| 17 | CH043L03 (1964) | 9648 | −92.82 | 48.76 | −9.99 | 13.63 |

**Table 6.** The statistics of the differences between the entire shipborne dataset and the reference gravity models; units [mGal].

| | | | Statistics of residuals | | | |
|---|---|---|---|---|---|---|
| Gravity model | Type | No. of data | Min | Max | Mean | STD |
| GO_CONS_GCF_2_TIM_R6 | GGM | 159924 | −770.16 | 873.92 | −8.35 | 31.06 |
| XGM2019e | GGM | 159924 | −766.38 | 886.17 | −2.80 | 13.68 |
| SSv29.1 | Altimetry | 159924 | −772.08 | 886.41 | −1.39 | 13.33 |
| DTU17 | Altimetry | 159924 | −771.21 | 885.12 | −1.70 | 12.95 |

height (SSH) which reveals a good performance over shallow water and near coastal areas as mentioned before.

It must be taken into consideration that the study area, especially the Red Sea region (where about 85% of the collected shipborne data around Egypt exit), is quite shallow with about 40% of depths less than 100 m and about 25% of depths less than 50 m (Rasul, Stewart, and Nawab 2015), the condition in which the altimetric observations degrades. On the other hand, the shipborne data revealed a bad performance in the cross-over adjustment (Denker and Roland 2005). Consequently, it is not clear whether DTU17 gravity grid or shipborne gravity data are better over the study area. So, precautions have to be taken before integrating such data, and this what will be discussed in the following section.

## Filtering shipborne data

### *Pre-refinement of shipborne data*

After the evaluation process, surveys no 7, 8, 16, and 17 demonstrated a not-good performance when compared with DTU17 giving a STD of more than 10 mGal (see Table 5). This is due to some extreme values of the

**Table 7.** The statistics of the differences between ship marine surveys and DTU17 after the pre-refinement process; units [mGal].

| | | | | Statistics of residuals | | | |
|---|---|---|---|---|---|---|---|
| Survey no | Survey name | No. of outliers | No. of remaining data | Min | Max | Mean | STD |
| 1 | 88004311 (1988) | 90 | 27256 | −19.98 | 19.48 | −4.11 | 3.06 |
| 2 | RC2507 (1984) | 312 | 38617 | −19.99 | 20.00 | 0.11 | 5.36 |
| 3 | 83005811 (1983) | 61 | 7500 | −18.86 | 19.98 | −0.57 | 4.67 |
| 4 | 83005911 (1983) | 261 | 7014 | −19.96 | 19.84 | −6.18 | 5.72 |
| 5 | 83008011 (1983) | 712 | 12735 | −20.00 | 19.82 | −9.36 | 5.09 |
| 6 | AKU30A (1979) | 134 | 708 | −19.98 | 15.31 | −9.65 | 6.99 |
| 7 | DI103B (1979) | 192 | 2101 | −11.05 | 19.99 | 9.29 | 5.95 |
| 8 | SHA1079 (1979) | 169 | 12025 | −19.84 | 19.98 | 1.63 | 6.05 |
| 9 | A2093L19 (1977) | 529 | 9109 | −19.94 | 19.98 | −2.49 | 6.95 |
| 10 | A2093L20 (1977) | 1 | 1498 | −17.30 | 19.92 | −1.41 | 5.32 |
| 11 | CH100L03 (1971) | 32 | 4064 | −19.92 | 19.96 | 1.61 | 5.03 |
| 12 | CH061L01 (1966) | 651 | 13297 | −19.93 | 19.97 | 4.94 | 6.66 |
| 13 | CH061L02 (1966) | 935 | 5871 | −19.52 | 19.99 | 8.85 | 6.64 |
| 14 | RC0911A (1965) | 13 | 739 | −19.97 | 11.83 | −5.62 | 6.03 |
| 15 | RC0911B (1965) | 6 | 961 | −19.64 | 19.78 | −2.65 | 5.12 |
| 16 | CH043L01 (1964) | 568 | 3230 | −19.98 | 19.76 | −6.88 | 7.00 |
| 17 | CH043L03 (1964) | 1859 | 7789 | −19.99 | 19.96 | −5.35 | 7.77 |
| Total data | | 6525 | 153489 | −20.00 | 20.00 | −1.34 | 7.11 |

gravity residuals in such surveys (>700 mGal in magnitude). A pre-refinement of shipborne gravity data is done for each survey according to DTU17 with a rigorous condition, in which the points with residuals more than 20 mGal in magnitude are considered as outliers and have been removed from the dataset. The value of 20 mGal is based on practical experience (Denker and Roland 2005; Featherstone 2009). A number of 6525 points have been removed from the dataset in this process. Table 7 shows the statistics of the residuals between the gravity observations of each survey and DTU17 after eliminating the outliers. Thereupon, all surveys revealed good results with max STD of 7.77 mGal for survey no 17 and max mean of 9.56 mGal in magnitude for survey no 6. Thus, all ship marine surveys are accepted and can be utilized. After the removal of 1025 duplicated points, the mean and STD of the remaining pre-refined 153489 points were −1.34 mGal and 7.11 mGal, respectively.

### *Refinement of shipborne data*

To make certain that the remaining shipborne gravity data are reliable and fully free from outliers, The cross-validation approach is applied (Kiamehr 2007). It is an appropriate approach for the detection and removal of gross errors that contaminate the shipborne dataset (Tscherning 1991).

### *Cross-validation approach*

For N observation locations in the shipborne gravity dataset (Kiamehr 2007), the first observation is excluded from the dataset then the value is

interpolated at such location using the remaining data and the specified interpolation algorithm. The known observation value is used for validation, i.e., computing the interpolation error (residual) at such a location as:

$$\text{Residual} = \text{interpolated value} - \text{observed value}$$

Then the excluded observation is put back into the dataset and the second observation is excluded. The value is interpolated at the second location using the remaining dataset (including the first observation) and the specified interpolation algorithm. Then the interpolation error at such location is computed as stated before. The second observation is put back into the dataset and this process is continued up to N times resulting in N interpolation errors. STD of the resulting residuals can be computed and help in detecting the outliers needed to be removed.

Thus, detecting and removing the outliers using the cross-validation approach can be summarized as follows:

1. select the suitable interpolation algorithm.
2. interpolate the value at each observation location, using the selected algorithm and the dataset (excluding the observation value at such location).
3. at each observation location, compute the residual.
4. compute the STD of the residuals and remove the outliers.

The quality of the cross-validation approach is affected by two factors, the selected interpolation algorithm and the locations of the validated points (Zaki et al. 2018). The best interpolation algorithm is the one that gives minimum STD of the differences between estimated and observed values (Kiamehr 2007). In this investigation, the kriging interpolation algorithm is used (Wackemagel 2013). Such an algorithm is known to be the best linear unbiased estimator (Matheron 1963). It is a very flexible gridding method that can be custom-fit to a dataset by specifying the proper variogram. Therefore, kriging with a linear variogram has been chosen as an appropriate interpolation algorithm to give the minimum interpolation error (Kiamehr 2007; Tscherning 1991).

### *Numerical analysis*

Within the study area ($20 \leq \text{lat} \leq 34$; $22 \leq \text{long} \leq 39$), a total number of 87709 points were deducted from the pre-filtered shipborne gravity data (see Figure 3). Then, the cross-validation approach is applied, and the STD of the residuals is computed. This process is repeated until the STD of the residuals is smaller than 1 mGal. The value 1 mGal is chosen as a strict

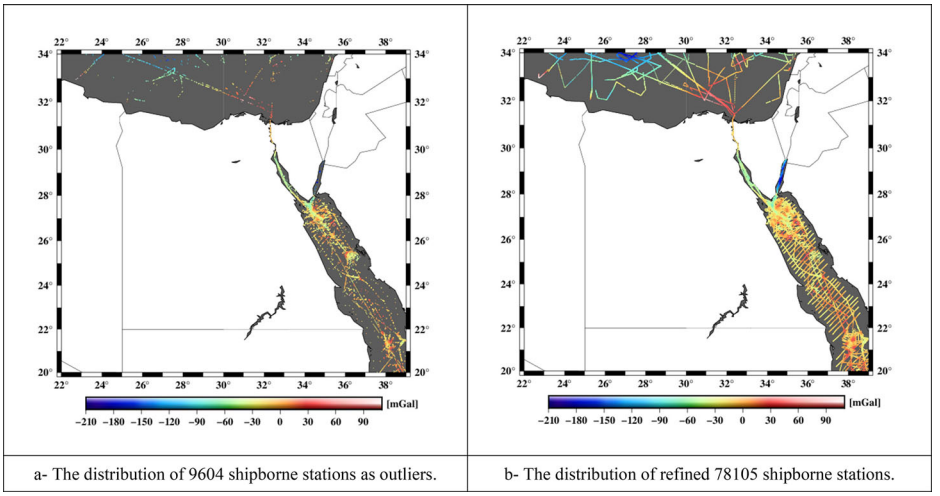


a- The distribution of 9604 shipborne stations as outliers.

b- The distribution of refined 78105 shipborne stations.

**Figure 4.** The distribution of 87709 shipborne stations after the refinement process; units [mGal]. Source: Author.

**Table 8.** The statistics of shipborne gravity data before and after applying cross-validation approach; units [mGal].

| Data type | No. of data | Min | Max | Mean | STD |
|---|---|---|---|---|---|
| Before full refinement | 87709 | −201.30 | 101.30 | −29.25 | 38.81 |
| After full refinement | 78105 | −201.30 | 97.30 | −30.16 | 39.71 |
| Residuals | 78105 | −3.12 | 3.12 | 0.01 | 0.97 |

condition to ensure that the remaining shipborne gravity data can be trusted. The points having differences greater than twice the STD are considered as outliers and are eliminated from the dataset (Zaki et al. 2018). This process results in eliminating a total number of 9604 points (10.95% of the total dataset) after only two iterations of applying the cross-validation approach, which in turn reflects the good work done in the pre-refinement process. Figure 4 presents the distribution of the removed outliers (panel a) and the remaining filtered data (panel b). The statistics of the shipborne gravity data before and after applying such a refinement are reviewed in Table 8. While the histogram of the residuals after the full refinement process is shown in Figure 5. The residuals follow a normal distribution with a high index of precision, where about 99.42% of the filtered dataset have residuals lower than 3 mGal in magnitude and about 76.47% of the filtered dataset have residuals lower than 1 mGal in magnitude.

## Integration of DTU17 grid and refined shipborne data

To create a fully consistent and reliable marine gravity field over the study area, the least-squares collocation (LSC) algorithm (Moritz 1980) is an appropriate technique to combine the filtered shipborne gravity data with

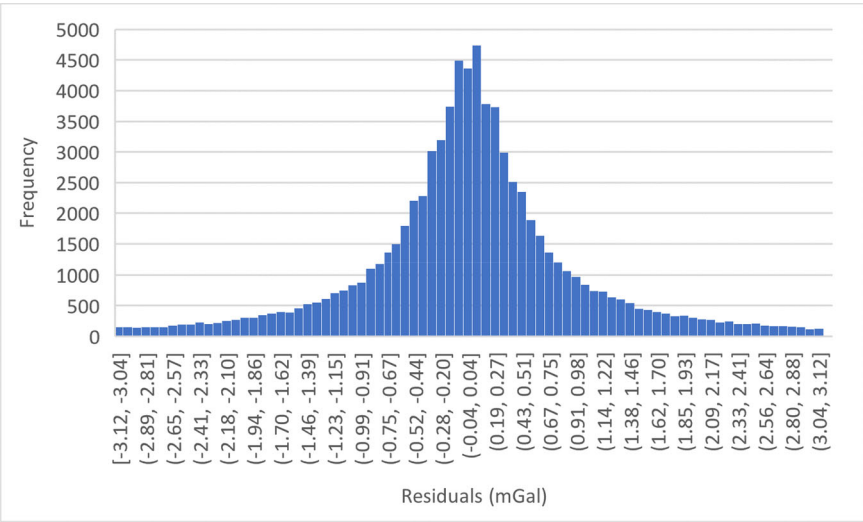


**Figure 5.** Histogram of the differences between observed and estimated free-air gravity anomalies after removing outliers.

the DTU17 grid (Strykowski and Forsberg 1998). LSC algorithm is a statistical estimator that combines least-squares adjustment and least-squares prediction in a form of a linear regression model (Zaki et al. 2018). Hence, applying the LSC will permit to statistically estimate the gravitational field by integrating heterogeneous gravity datasets from different sources. At any arbitrary point P, the predicted value of the gravity anomaly $(S_p)$ is given in Eq. 1.

$$S_p = C_{Pl} C_{ll}^{-1} L \quad [1]$$

Where $C_{ll}$ is the covariance matrix of the gravity measurements and $C_{Pl}$ denotes the cross-covariance vector between the estimated signal and the measurements.

Firstly, the residuals between the refined shipborne gravity data and the DTU17 are computed. Then, LSC is applied to grid the resultant residuals. To be able to combine the two gravity datasets, the residuals are gridded onto a regular mesh of 1 arc-minute resolution, the same resolution of the DTU17 grid.

Thereupon, a second-order Markov covariance model (Eq. 2) was applied with a 30-km correlation length and a white-noise of 1 mGal.

$$C(S) = C_0(1 + \alpha S)\square^{-\alpha S} \quad [2]$$

where $C_0$ denotes the empirical variance, $\alpha$ is the correlation length parameter, and S stands for the distance between the couple of points under consideration. The parameters of the model were optimized by testing them over a range of 10–50 km and 1–5 mGal (Zaki et al. 2018). Finally, the grid of the

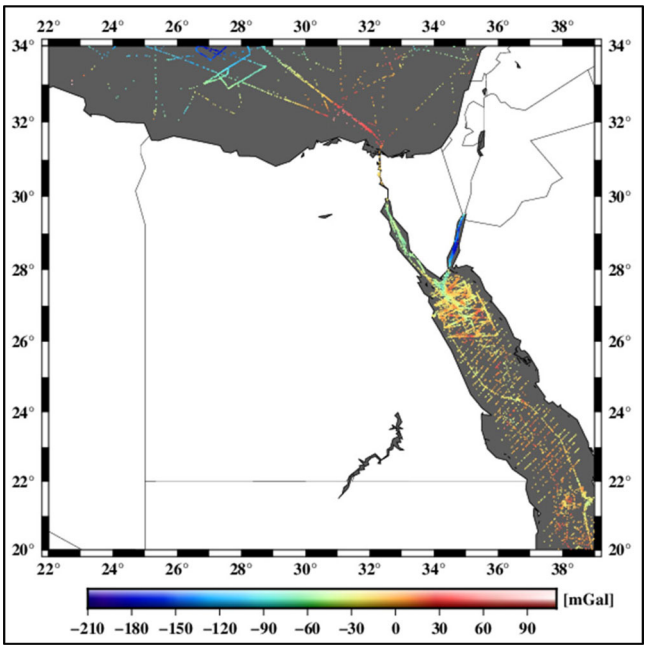


**Figure 6.** The distribution of 8000 testing shipborne stations; units [mGal]. Source: Author.

residuals is added to the pre-gridded DTU17. This process in turn showed an enhancement of the DTU17 grid as discussed in the following section.

### *Testing the final marine gravity map*

The final marine gravity map was tested using 8000 randomly chosen shipborne sparse gravity stations (∼10% of the dataset) (see Figure 6), that were not included when applying LSC. The comparison between the 8000 extracted shipborne observations and the DTU17 before and after the integration process reflects the enhancement gained by using the LSC algorithm as shown in Table 9. Where the mean dropped from 1.10 mGal to 0.12 mGal in magnitude and the STD dropped from 6.50 mGal to 2.03 mGal.

On the other hand, Table 10 shows the comparison between the entire refined shipborne dataset and the DTU17 before and after the integration process. Both the mean and the STD dropped from −1.28 to −0.08 mGal and from 6.49 to 1.98 mGal, respectively, which reveals a significant enhancement of the final grid.

## Conclusion

After the evaluation of the shipborne dataset by the four gravity models, DTU17 altimetry-derived gravity grid is chosen to be integrated with the shipborne gravity dataset for two reasons: the first is the low value of the

**Table 9.** The statistics of the differences between 8000 randomly chosen shipborne stations and DTU17 before and after the integration process; units [mGal].

| | Statistics of residuals | | | |
|---|---|---|---|---|
| Integration | Min | Max | Mean | STD |
| Before | −20.31 | 20.10 | −1.10 | 6.50 |
| After | −13.43 | 18.68 | 0.12 | 2.03 |

**Table 10.** The statistics of the differences between 70105 shipborne stations and DTU17 before and after the integration process; units [mGal].

| | Statistics of residuals | | | |
|---|---|---|---|---|
| Integration | Min | Max | Mean | STD |
| Before | −20.51 | 20.65 | −1.28 | 6.49 |
| After | −17.47 | 20.49 | −0.08 | 1.98 |

STD of the residuals with the shipborne data (12.95 mGal) compared to the results from other gravity models. And the second is the algorithm employed to acquire the gravity data from altimetric observations, i.e., sea surface height (SSH) which reveals a good performance over shallow water and near coastal areas (the condition in the study area). The pre-refinement step showed that all ship marine surveys are accepted and can be utilized, where the mean and STD of the remaining shipborne gravity dataset become −1.34 mGal and 7.11 mGal, respectively, after the removal of 6525 points as outliers (having a STD $>$ 20 mGal in magnitude). 87709 points were deducted from the pre-filtered shipborne dataset to fit the study area and the cross-validation approach with the kriging interpolation algorithm were applied two times until the STD of the differences between the observed and the estimated gravity anomalies reach a value less than 1 mGal. In this step, 10.95% of the shipborne dataset were eliminated. Finally, the refined shipborne gravity data were gridded onto a 1 min-resolution mesh to fit the DTU17 grid using the LSC technique and then added to the pre-gridded DTU17. The comparison between the filtered shipborne dataset and the DTU17 before and after the integration process revealed the significant enhancement gained from the final marine gravity map where both the mean and the STD dropped from −1.28 to −0.08 mGal and from 6.49 to 1.98 mGal, respectively.

## Disclosure statement

No potential conflict of interest was reported by the authors.

## ORCID

Ahmed Zaki http://orcid.org/0000-0002-2709-5551
Mahmoud Magdy http://orcid.org/0000-0003-0090-8097

## References


Andersen, O. B., and P. Knudsen. 2019. The DTU17 global marine gravity field: First validation results. *International Association of Geodesy Symposia*:83–7.

Andersen, O. B., P. Knudsen, and P. A. Berry. 2010. The DNSC08GRA global marine gravity field from double retracked satellite altimetry. *Journal of Geodesy* 84 (3):191–9..

Andersen, O. B., P. Knudsen, S. Kenyon, J. Factor, and S. Holmes. 2013. The DTU13 Global marine gravity field—first evaluation. In *Ocean surface topography science team meeting*. Boulder, C*olorado*.

Brockmann, J. M., T. Schubert, T. Mayer-Gürr, and W.-D. Schuh. 2019. The Earth's gravity field as seen by the GOCE satellite - an improved sixth release derived with the time-wise approach (GO_CONS_GCF_2_TIM_R6). *GFZ Data Services*. https://doi.org/10.5880/ICGEM.2019.003

Brockmann, J. M., T. Schubert, and W. Schuh. 2021. An improved model of the earth's static gravity field solely derived from reprocessed GOCE data. *Surveys in Geophysics* 42 (2):277–316..

Christensen, A. N., and O. B. Andersen. 2016. Comparison of satellite altimetric gravity and ship-borne gravity - Offshore Western Australia. *ASEG Extended Abstracts* 2016 (1): 1–5..

Denker, H., and M. Roland. 2005. Compilation and evaluation of a consistent marine gravity data set surrounding Europe. In *A window on the future of geodesy*, 248–53. Berlin, Heidelberg: Springer. https://doi.org/10.1007/3-540-27432-4_42

Drinkwater, M. R., R. Floberghagen, R. Haagmans, D. Muzi, and A. Popescu. 2003. GOCE: ESA's first earth explorer core mission. *Space Science Reviews* 108 (1/2):419–32..

Fairhead, J. D., C. M. Green, and M. E. Odegard. 2001. Satellite-derived gravity having an impact on marine exploration. *The Leading EDGE* 20 (8):873–6..

Featherstone, W. E. 2009. Only use ship-track gravity data with caution: A case-study around Australia. *Australian Journal of Earth Sciences* 56 (2):195–9..

Förste, C., S. L. Bruinsma, O. Abrikosov, J.-M. Lemoine, T. Schaller, H.-J. Götze, J. Ebbing, J. C. Marty, F. Flechtner, G. Balmino, et al. 2014. EIGEN-6C4 The latest combined global gravity field model including GOCE data up to degree and order 2190 of GFZ Postdam and GRGS Toulouse. *GFZ Data Services*. https://doi.org/10.5880/icgem.2015.1

Gaina, C., W. R. Roest, R. D. Müller, and P. Symonds. 1998. The opening of the Tasman Sea: A gravity anomaly animation. *Earth Interactions* 2 (4):1–23.

Gilardoni, M., M. Reguzzoni, and D. Sampietro. 2016. GECO: A global gravity model by locally combining GOCE data and EGM2008. *Studia Geophysica et Geodaetica* 60 (2): 228–47..

Hackney, R. I., and W. E. Featherstone. 2003. Geodetic versus geophysical perspectives of the 'gravity anomaly. *Geophysical Journal International* 154 (1):35–43..

Haxby, W. F., G. D. Karner, J. L. LaBrecqu, and J. K. Weisse. 1983. Digital images of combined oceanic and continental data sets and their use in tectonic studies. *Eos, Transactions American Geophysical Union* 64 (52):995–1004..

Hofmann, B., and W. H. Moritz. 2006. *Physical geodesy*. Vienna: Springer.

Ince, E. S., F. Barthelmes, S. Reißland, K. Elger, C. Förste, F. Flechtner, and H. Schuh. 2019. ICGEM – 15 years of successful collection and distribution of global gravitational models, associated services, and future plans. *Earth System Science Data* 11 (2):647–74..

Kiamehr, R. 2007. Qualification and refinement of the gravity database based on cross-validation approach - A case study of Iran. *Acta Geodaetica et Geophysica Hungarica* 42 (3):285–95..

Kvas, A., J. M. Brockmann, S. Krauss, T. Schubert, T. Gruber, U. Meyer, T. Mayer-Gürr, W. D. Schuh, A. Jäggi, and R. Pail. 2021. GOCO06s- A satellite-only global gravity field model. *Earth System Science Data* 13 (1):99–118..

Liu, L., X. Jiang, S. Liu, L. Zheng, J. Zang, X. Zhang, and L. Liu. 2016. Calculating the marine gravity anomaly of the South China sea based on the inverse stokes formula. *IOP Conference Series: Earth and Environmental Science* 46:012062.

Matheron, G. 1963. Principles of geostatistics. *Economic Geology* 58 (8):1246–66..

Moritz, H. 1980. *Advanced physical geodesy*. Tunbridge, England: Karlsruhe: Wichmann.

Omar, K. M., S. Ses, and A. Mohamed. 2005. *Enhancement of Height System For Malaysia Using Space Technology: The Study of the Datum Bias Inconsistencies in Peninsular Malaysia*. Faculty of Geoinformation Science and Engineering Universiti Teknologi Malaysia.

Pail, R., S. Bruinsma, F. Migliaccio, C. Förste, H. Goiginger, W. D. Schuh, E. Höck, M. Reguzzoni, J. M. Brockmann, O. Abrikosov, et al. 2011. First GOCE gravity field models derived by three different approaches. *Journal of Geodesy* 85 (11):819–43..

Pail, R., T. Fecher, D. Barnes, J. F. Factor, S. A. Holmes, T. Gruber, and P. Zingerle. 2018. Short note: The experimental geopotential model XGM2016. *Journal of Geodesy* 92 (4): 443–51..

Pavlis, N. K., S. A. Holmes, S. C. Kenyon, and J. K. Factor. 2012. The development and evaluation of the Earth Gravitational Model 2008 (EGM2008). *Journal of Geophysical Research: Solid Earth* 117 (B4):n/a–/a..

Rasul, N. M. A., I. C. F. Stewart, and Z. A. Nawab. 2015. Introduction to the red sea: Its origin, structure, and environment. In *The Red Sea: The formation, morphology, oceanography and environment of a young ocean basin*, 1–28. Berlin, Heidelberg: Springer. https://doi.org/10.1007/978-3-662-45201-1

Rexer, M., C. Hirt, and R. Pail. 2017. High-resolution global forward modelling: A degree-5480 global ellipsoidal topographic potential model. In EGU General Assembly Conference Abstracts (Vol. 19, p. 7725). https://ui.adsabs.harvard.edu/abs/2017EGUGA.19.7725R/abstract.

Rudolph, S., J. Kusche, and K. H. Ilk. 2002. Investigations on the polar gap problem in ESA's gravity field and steady-state ocean circulation explorer mission (GOCE). *Journal of Geodynamics* 33 (1–2):65–74..

Sandwell, D. T., E. Garcia, K. Soofi, P. Wessel, M. Chandler, and W. H. F. Smith. 2013. Toward 1-mGal accuracy in global marine gravity from CryoSat-2, Envisat, and Jason-1. *The Leading Edge* 32 (8):892–9..

Sandwell, D. T., H. Harper, B. Tozer, and W. H. F. Smith. 2021. Gravity field recovery from geodetic altimeter missions. *Advances in Space Research* 68 (2):1059–72..

Sandwell, D. T., R. D. Müller, W. H. Smith, E. Garcia, and R. Francis. 2014. Marine geophysics. New global marine gravity model from CryoSat-2 and Jason-1 reveals buried tectonic structure. *Science (New York, NY)* 346 (6205):65–7..

Sandwell, D. T., and W. H. Smith. 1997. Marine gravity anomaly from Geosat and ERS 1 satellite altimetry. *Journal of Geophysical Research: Solid Earth* 102 (B5):10039–54..

Sandwell, D. T., W. H. Smith, S. Gille, S. Jayne, K. Soofi, and B. Coakley. 2001. Bathymetry from space. In *Report of the high-resolution ocean topography science working group meeting*, ed. D. B. Chelton, 87–108. Oregon State University, College of Oceanic and Atmospheric Sciences.

Sneeuw, N., and M. van Gelderen. 1997. The polar gap. In *Geodetic boundary value problems in view of the one centimeter geoid*, 559–68. Berlin, Heidelberg: Springer. https://doi.org/10.1007/bfb0011717

Strykowski, G., and R. Forsberg. 1998. operational merging of satellite, airborne and surface gravity data by draping techniques. In *Geodesy on the move*, 243–8. Berlin, Heidelberg: Springer. https://doi.org/10.1007/978-3-642-72245-5_35

Tscherning, C. C. 1991. A strategy for gross-error detection in satellite altimeter data applied in the baltic-sea area for enhanced geoid and gravity determination. In *Determination of the geoid: Present and future*, 95–107. New York, NY: Springer. https://doi.org/10.1007/978-1-4612-3104-2_12

Wackemagel, H. 2013. *Multivariable geostatistics: An introduction with applications*. Berlin Heidelberg: Springer-Verlag. https://doi.org/10.1007/978-3-662-05294-5

Wei, L., X. Xinyu, L. Jiancheng, and Z. Guangbin. 2018. The determination of an ultra-high gravity field model SGG-UGM-1 by combining EGM2008 gravity anomaly and GOCE observation data. *Acta Geodaetica et Cartographica Sinica* 47 (4):425–34..

Wessel, P., and A. B. Watts. 1988. On the accuracy of marine gravity measurements. *Journal of Geophysical Research: Solid Earth* 93 (B1):393–413..

Zaki, A., A. H. Mansi, M. Selim, M. Rabah, and G. El-Fiky. 2018. Comparison of satellite altimetric gravity and global geopotential models with shipborne gravity in the Red Sea. *Marine Geodesy* 41 (3):258–69..

Zaki, A., and S. Mogren. 2021. A high-resolution gravimetric geoid model for Kingdom of Saudi Arabia. *Survey Review*:1–16. https://doi.org/10.1080/00396265.2021.1944544.

Zhang, S., A. Abulaitijiang, O. B. Andersen, D. T. Sandwell, and J. R. Beale. 2021. Comparison and evaluation of high-resolution marine gravity recovery via sea surface heights or sea surface slopes. *Journal of Geodesy* 95 (6):1–17..

Zhang, Y., J. Zhang, Y. Ji, and H. Zhang. 2003. Calculation of geoid undulations and gravity anomalies in the South China Sea by using the TOPEX/Poseidon and geosat altimeter data. In *Ocean remote sensing and applications*, ed. R. J. Frouin, Y. Yuan, and H. Kawamura, Vol. 4892, 521–8.

Zingerle, P., R. Pail, T. Gruber, and X. Oikonomidou. 2020. The combined global gravity field model XGM2019e. *Journal of Geodesy* 94 (7):1–12..